FRONTIERS OF PHYSICS

RESEARCH ARTICLE
Volume 21 / Issue 11 / 113201 / 2026

Identification of quantum generative circuits with parallel quantum neural network

Zheping Wu [1], Xiaopeng Huang [2], Hengyue Jia [3], Haobin Shi [1], Wei-Wei Zhang [1,†]

1 School of Computer Science, Northwestern Polytechnical University, Xi'an 710129, China
2 school of cybersecurity, Northwestern Polytechnical University, Xi'an 710129, China
3 School of Information, Central University of Finance and Economics, Beijing 100081, China
Corresponding author. E-mail: †wei-wei.zhang@nwpu.edu.cn
Received December 20, 2025; accepted March 3, 2026

ABSTRACT

The rapid emergence of quantum technology has raised new challenges in distinguishing various quantum circuits of similar functions. In this work, we propose parallel quantum embedding neural network (ParaQuanNet) for the efficient identification of quantum generative circuits via classifications of the corresponding output data. Specifically, we generated W-like states with eight generative quantum circuits realizing the generative quantum denoising diffusion probabilistic models (QDDPM). Our ParaQuanNet can classify these eight classes of generated quantum data with an accuracy of 99.5%, even though all of them are trained to generate the same types of quantum data. With a novel design of parallel quantum embedding unit (PQEU) in our neural networks, our ParaQuanNet enables the quantum kernel circuit parallelly process all the receptive fields of quantum data, which empowers the quantum data processing efficiency. We also integrate the mutual unbiased measurements into our ParaQuanNet and further improve its performance. We apply our ParaQuanNet on the classification of classical data sets and demonstrate a good performance of quantum neural networks on these tasks. Our approach demonstrates good robustness to noisy data and the circuit-level noise with a Python realization in calssical GPU. Our results highlight ParaQuanNet as a scalable and effective framework for quantum circuits identification, contributing to the broader development of quantum machine intelligence.

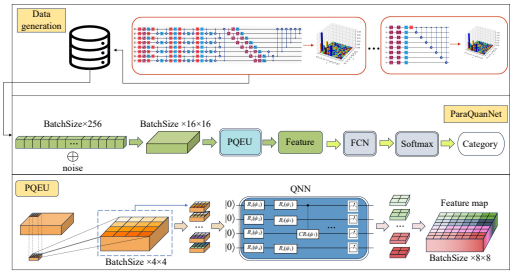

Keywords quantum machine learning, quantum data generation, quantum classification

1 Introduction

Quantum technology has attracted tremendous attention around the world and has been recognized as the height of the next information revolution. Within recent years, quantum technology has demonstrated breakthroughs in communications [1–3], quantum computations [4–7], quantum simulations [8–13] and quantum metrology [14–17]. With the promising quantum advantages demonstrated, quantum technology is still at the stage of near term Noisy Intermediate-Scale Quantum era and there are still challenges in the field to find more practical applications for current quantum technologies [18, 19].

In the meantime, the development of artificial intelli-

arXiv: 2603.02834v1
https://doi.org/10.15302/frontphys.2026.113201

gence is also rising, showcasing its power in the emergence of intelligence [20–22]. Recent advances in large-scale deep learning —particularly transformer-based architectures have led to the development of models exhibiting emergent cognitive capabilities that were neither explicitly programmed nor anticipated at smaller scales [23, 24]. These behaviors include in-context learning, abstract reasoning, and multimodal integration, suggesting the spontaneous organization of representational hierarchies akin to elements of natural cognition [25].

While the artificial intelligence is developing extremely fast, the corresponding computational power cost also grows vastly [26]. Attracted by the demonstrated computational advantage of quantum technology and inspired by the development of artificial intelligence, scholars in the quantum field explore the power of quantum artificial intelligence. One direction aligning with this direction is the quantum variational algorithms for the optimization problems [27, 28], which are quantum-classical hybrid algorithms. The other direction is the exploration of the advantages of quantum artificial intelligence, such as the quantum ability in data mining [12], classifications [29, 30] and data generation [31–33]. The quantum data generation varies in two ways, one is the generation of quantum representations of classical data, such as the MNIST data [31–33]. The other way is the generation of quantum states, such as quantum entangled states like GHZ and W states [34–36], and quantum multi-particle interaction systems [37, 38]. There are also efforts to develop the structure of quantum neural networks [39, 40].

In this work, we focus on the aspect of copyright authentication in quantum artificial intelligence to advance the field of quantum AI further. We propose a method for the identification of quantum generative circuits with our novel parallel quantum embedding neural network (ParaQuanNet). Specifically, we identify the quantum generative circuits by the classifications of the quantum AI generated data from these quantum generative circuits. We introduce the mutual unbiased measurements into our ParaQuanNet to further improve the classification accuracy. Our results highlight ParaQuanNet as a scalable and effective framework for quantum circuits identification, contributing to the broader development of quantum machine intelligence. Our contributions are as follows:

- We forward the quantum artificial generation field for counterfeit tracking and copyright protection by identifying the quantum AI-generated data/classifying the quantum generative circuits, which can also be used to classify classical data.
- We propose a parallel quantum embedding neural network (ParaQuanNet) enabling the implementation of the quantum convolution operations in parallel.
- We design a parallel quantum embedding unit (PQEU) by utilizing a shared QNN as its kernel, and achieve parameter sharing advantages that significantly decrease model complexity while enhancing both training efficiency and generalization performance.
- We integrate two types of mutual unbiased measurements into our ParaQuanNet, which further improves the classification accuracy.
- Our ParaQuanNet demonstrates the better robustness to quantum-specified data noise and circuit level noise compared with the traditional quantum convolution neural network.

2 Quantum generative circuits identification with parallel quantum neural network

This work aims to identify which quantum AI generative circuits are the quantum states generated from and therefore to distinguish the quantum generative circuits. In this section, we propose a parallel quantum embedding neural network (ParaQuanNet) architecture for the efficient quantum generative circuits identification. Specifically, we will introduce the generative circuits we used as demonstration in this works, the construction of ParaQuanNet and its core part of parallel quantum embedding network, the novel integration of mutual unbiased measurement in our quantum ParaQuanNet, and our main results of quantum generative circuits identificaiton.

The architecture of our Parallel quantum neural network is shown in Fig. 1, and it consists of three parts, the data generated process, the quantum neural networks and the measurements. In the data generation process, we collect the quantum data from various quantum generative circuits which are trained to generate the same types of data. In our demonstration, we identify 8 types of quantum generative circuits. The quantum neural networks we design include a parallel quantum embedding network and enable the parallel quantum convolution. We integrate the mutual unbiased measurements into our quantum neural networks to improve the performance further.

2.1 Quantum generative circuits

The data in our proposal is generated with various quantum generative circuits which are trained by following a quantum denoising diffusion probabilistic process [20, 34–36]. Specifically, quantum diffusion model extends classical denoising diffusion probabilistic models (DDPMs) into the domain of quantum states by replacing Gaussian noise with quantum channels and learning to reverse this noise process using quantum neural networks. A practical effective architecture for this task

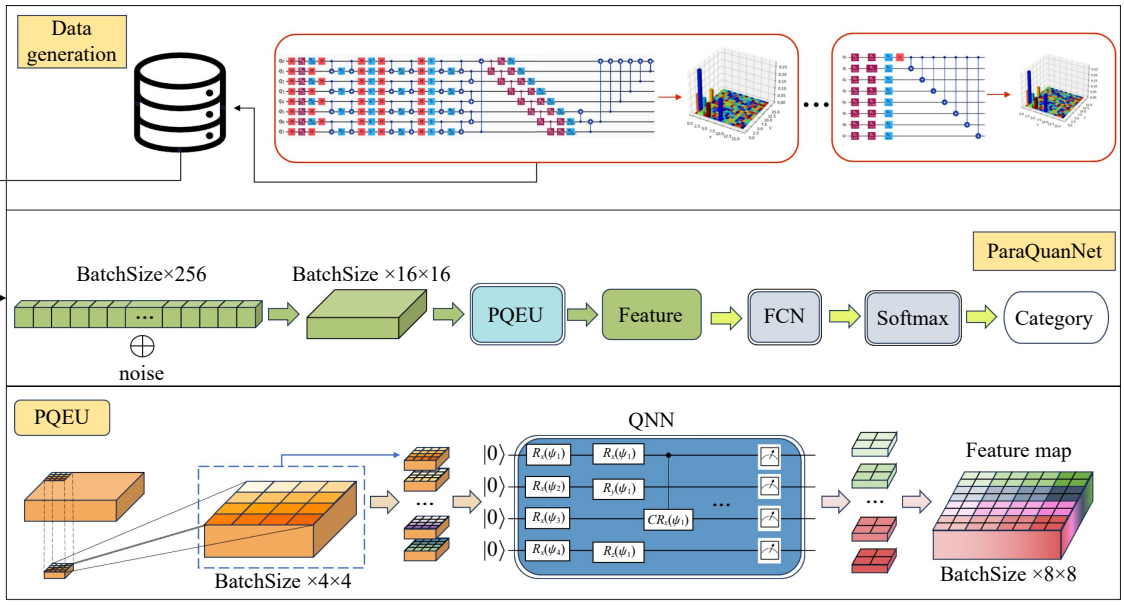

Fig. 1 Sketch of our scheme for quantum identification of quantum AI-generated data. Top: The quantum data generated from various quantum generative circuits. Middle: The workflow of our ParaQuanNet. Bottom: The structure of the proposed PQEU.

is the quantum U-Net in Ref. [34], a quantum analogue of the classical U-Net that uses hierarchical encoding and decoding with skip connections to preserve multiscale structure in quantum data. In a quantum DDPM with a quantum U-Net, the forward process gradually perturbs an initial quantum state through controlled CPTP noise channels, while the quantum U-Net learns the reverse transitions by predicting and removing the injected quantum noise at each diffusion step. This combination provides a powerful framework for quantum state reconstruction, generation, and noise mitigation, leveraging the expressive capacity of quantum circuits to capture both local and global correlations that arise in many-body quantum systems.

In this work, we design various neural network architectures and train these neural networks to generate the same kind of quantum data, i.e., the previously defined W-like state, which is defined as follows:

$$\begin{aligned}\widetilde{W} = {} & \alpha_1|10000000\rangle + \alpha_2|01000000\rangle \\ & + \alpha_3|00100000\rangle + \alpha_4|00010000\rangle \\ & + \alpha_5|00001000\rangle + \alpha_6|00000100\rangle \\ & + \alpha_7|00000010\rangle + \alpha_8|00000001\rangle, \end{aligned} \tag{1}$$

with $\alpha_i, i \in [1, \cdots, 8]$ as complex numbers and $\sum_i |\alpha_i|^2 = 1$. We define the success rate of generations is

$$\begin{aligned}P^W_{\boldsymbol{succ}} = {} & P_{10000000} + P_{01000000} \\ & + P_{00100000} + P_{00010000} \\ & + P_{00001000} + P_{00000100} \\ & + P_{00000010} + P_{00000001}. \end{aligned} \tag{2}$$

Here $P_{10000000}$, $P_{01000000}$, $P_{00100000}$, $P_{00010000}$, $P_{00001000}$, $P_{00000100}$, $P_{00000010}$ and $P_{00000001}$ are the probabilities of the generated states project to the corresponding computation bases $\{|00000001\rangle, |00000010\rangle, |00000100\rangle, |00001000\rangle, |00010000\rangle, |00100000\rangle, |01000000\rangle, |10000000\rangle\}$.

Specifically, in our demonstrations we design 8 various generative circuits as shown in Fig. 2, where a convolution layer applies a single quasi-local unitary (U_i) in a translation invariant manner for finite depth, inspired by Ref. [41]. For pooling, a fraction of qubits are mathematically traced out temporally, and their states are stored and reused in the later coming layers. Therefore, the nonlinearities in our architectures arise from tracing out partial degrees of freedom. With these 8 well trained generative circuits, we generate 2000 data from each quantum generative circuits, and the success rate of the generations for each of these circuits are above 0.95. In our work, we will use our proposed parallel quantum embedding neural network to identify which of these generative circuits are the quantum data generated from.

2.2 Parallel quantum embedding network

In this work, we propose a parallel quantum embedding network for the efficient data processing in quantum neural networks (ParaQuanNet). Our novel parallel quantum computing unit (PQEU) is designed in our ParaQuanNet as shown at the bottom of Fig. 1, under the inspiration of the high efficiency of GPU parallel computing, i.e., SIMD (Single Instruction Multiple Data) architecture [42]. By leveraging parameter shar-

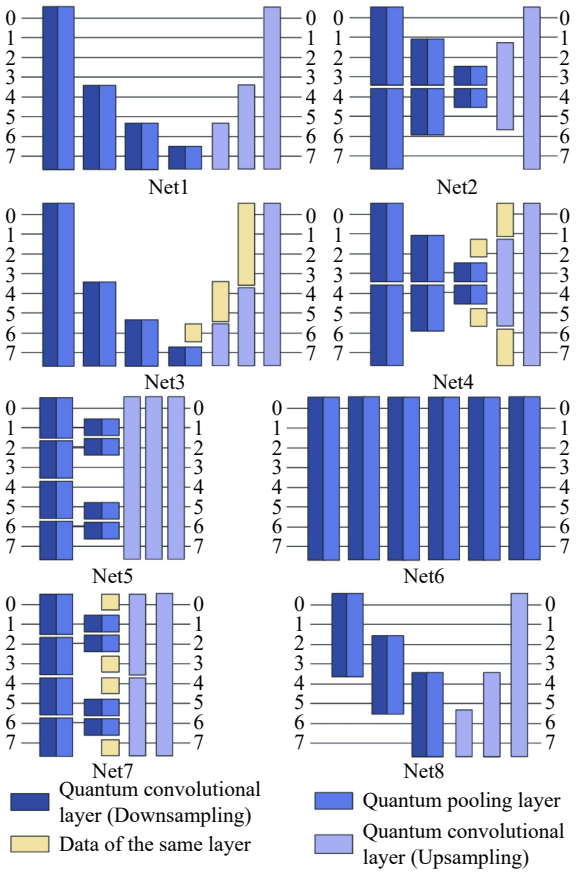

Fig. 2 The eight structures of quantum W-like states generation circuits used for our data generation.

ing, localized connectivity, and efficient lattice-based data processing, PQEU achieves stronger feature representation capabilities with fewer parameters and significantly accelerates the computational efficiency of quantum convolutional neural networks (QCNNs). Specifically, our ParaQuanNet consists of three components: data preprocessing, feature extraction via PQEU, feature fusion, and classification. Quantum-generated data, inherently represented as complex-valued vectors, and mapped into distinct 2D tensors. The restructured data is processed through independent PQEU blocks, enabling simultaneous extraction of localized quantum features while maintaining parameter efficiency through weight sharing. Extracted features are fused via entanglement-inspired aggregation before being classified using a fully connected network. A softmax-activated output layer generates probabilistic predictions for classifying quantum states.

During the training process, our data is reorganized in the following way. Firstly, the input quantum data $\boldsymbol{z} \in \boldsymbol{C}^{n\times 256}$ are reshaped into the size of $\mathcal{T} \in \boldsymbol{R}^{n\times 16\times 16}$, where n represents the batchsize, and the process is classical implemented in our simulations. Then, the processed data sets are fed into our shared-parameter PQEU

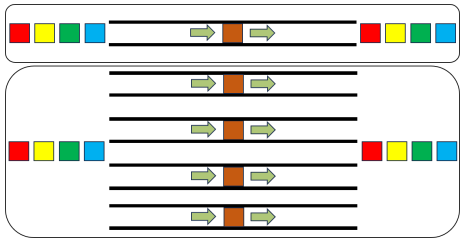

Fig. 3 Top: Convention quantum neural network data flow. Bottom: The sketch of our PQEU process data flow.

modules for the quantum feature extraction:

$$\boldsymbol{f}_* = \mathrm{PQEU}(\mathcal{T}; U(\theta)),$$

with $U(\theta)$ representing the quantum neural network in our PQEU. In the last step, the fused features are sent through a fully convolution network followed by Softmax activation, and output the final class identification category of the data.

The key innovation in our ParaQuanNet is the parallel quantum embedding unit (PQEU), which upgrades the traditional quantum convolution network by enabling the processing of multiple patches simultaneously and achieves both spatial feature extraction and computational acceleration as shown in Fig. 3. In our simulations, we realize it in GPU. While applying in quantum NISQ devices, it requires multi copies of trained PQEU for the process. The mechanism of our PQEU was invented under the inspiration of the SIMD (Single Instruction Multiple Data) architecture in classical parallel computing. The workflow of PQEU is shown at the bottom of Fig. 1. The structure of our QNN consists of the single qubit gates R_x, R_y, R_z, SX gate, Hadamard gates, and the two-qubit CNOT gates and controlled rotation gates CR_x, CR_y, CR_z. In the workflow of our PQEU, the first part is a data griding process, which converts the data with the size of $\mathrm{BatchSize} \times 16 \times 16$ into $16 \times \mathrm{BatchSize}$ pieces of the data with a size of 4×4. These $16 \times \mathrm{BatchSize}$ pieces of data are further vertically stacked for our 4-qubit convolution kernel quantum neural network (QNN). The output of the QNN is a vertically stacked feature with a size of 2×2, which is further fused into a feature map with a size of 8×8.

We summarize to emphasize the two critical innovations of our PQEU as follows.

- Batch Griding: Instead of processing patches sequentially, our PQEU converts a batch of 'patches' into a 4-qubit system, enabling simultaneous processing of multiple patches in one round of the QNN.
- Shared Parameter Convolution: All patches within a batch share identical parameterized quantum gates, reducing the number of circuit free parameters while maintaining spatial feature locality.

2.3 Mutual unbiased measurements empowered ParaQuanNet

In this section, we unleash quantum advantage for neural networks by introducing mutual unbiased measurement in two modes and experimentally demonstrate the great improvements of our framework in classification accuracy by the average improvement of 18.9% compared with the model with ordinary computational measurements.

Mutually unbiased bases (MUB) measurements are essential for quantum state tomography, as they use measurement bases that are maximally incompatible, meaning knowledge of a quantum state in one base reveals no information about its state in the others. By combining outcomes from these bases researchers can reconstruct a quantum state's full density matrix with optimal efficiency, minimizing redundancy and ensuring complete characterization. This approach is critical for verifying quantum systems in experiments, such as validating entangled states or calibrating qubits, as it maximizes information extraction while reducing measurement overhead [43–47]. Mathematically, a pair of MUBs as two orthonormal bases on a d-dimensional Hilbert space $\mathbb{C}^d$, namely, $\{|e_j\rangle\}_{j=1}^{d}$ and $\{|f_k\rangle\}_{k=1}^{d}$, with the property that $|\langle e_j|f_k\rangle|^2 = \frac{1}{d}$ for all j and k.

Specifically, we introduce mutually unbiased bases measurements in our ParaQuanNet to fully release quantum advantage and empower the learning efficiency and precision. For a single qubit with 2-dimensional Hilbert space, the three mutually unbiased bases are the Pauli X, Y, Z bases. The measurement operators for Pauli X, Y, Z bases are $\{\hat{\sigma}_x, \hat{\sigma}_y, \hat{\sigma}_z\}$ and the corresponding measurement bases are $\{|0\rangle, |1\rangle\}$ (computational bases), $\{|+\rangle = \frac{1}{\sqrt{2}}(|0\rangle + |1\rangle), |-\rangle = \frac{1}{\sqrt{2}}(|0\rangle - |1\rangle)\}$, $\{|R\rangle = \frac{1}{\sqrt{2}}(|0\rangle + \mathrm{i}|1\rangle), |L\rangle = \frac{1}{\sqrt{2}}(|0\rangle - \mathrm{i}|1\rangle)\}$. The key property is that the overlap between any two states from different bases is $|\langle\psi_i|\phi_j\rangle| = \frac{1}{\sqrt{2}}$, ensuring maximal uncertainty. To fully reconstruct a qubit's density matrix ρ, we need its projections onto these three bases, $\rho = \frac{1}{2}(I + \langle X\rangle X + \langle Y\rangle Y + \langle Z\rangle Z)$, where $\langle\hat{\sigma}\rangle_x, \langle\sigma\rangle_y, \langle\sigma\rangle_z$ are expectation values obtained by measuring in the X, Y, and Z bases. Each basis provides complementary information, Z basis reveals populations (diagonal elements of ρ), X/Y basis reveals coherence (off-diagonal elements). The completeness and minimal redundancy for learning the information of a qubit are guaranteed, since the three Pauli bases span the space of 2×2 Hermitian matrices, ensuring no missing information, and each measurement contributes unique, non-overlapping data.

For the measurement in our ParaQuanNet for classifications, we propose two frameworks of MUB measurement, namely, simultaneous MUB measurements (S-MUB) and alternating MUB measurements (A-MUB) as shown in Fig. 4. In S-MUB, the qubits in QCNN are measured in the three MUB simultaneously as shown in Fig. 4(a), the averaged measurement outcomes are used for the QCNN training. In A-SUB, the qubits in the QCNN are measured alternately in sequence by three MUBs (the timely order in our experiments are Pauli Z, Pauli X, Pauli Y) as shown in Fig. 4(b). Operationally, due to the disturbance from quantum measurement, quantum measurements are applied on multiple copies of the quantum states, and then we extract the statistical results from these sample measurements. Compared with Pauli Z measurements, S-MUB and A-MUB is more reflective quantum properties of quantum states and extract more information from measurements. Therefore, it will be shown in our simulations that the S-MUB and A-MUB will give higher classification accuracy compared with the Pauli Z.

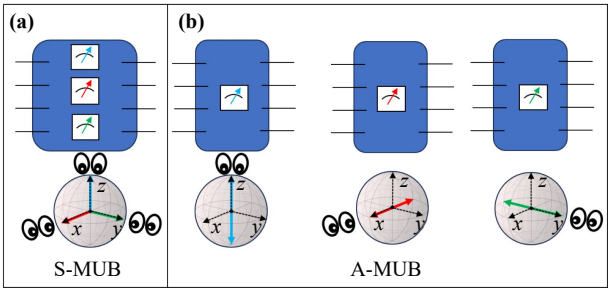

Fig. 4 Sketch of our two proposed measurement modes: **(a)** S-MUB and **(b)** A-MUB, where the eyes represent the quantum observations/measurements.

2.4 Quantum generative circuits identificaiton with our ParaQuanNet

In this study, we employ ParaQuanNet to characterize quantum generative circuits by classifying the data produced by those circuits. Through this classification-based approach, our framework effectively links the structure of each quantum generative model to the statistical properties of its output, enabling a systematic identification of the underlying generative mechanisms. The pseudocode of our algorithm is shown in Fig. 1. All of our results are simulated in classical computer.

For the eight groups of W-like states generated the eight quantum generative circuits in Fig. 2, the classification accuracy reaches 99.5% with A-MUB or S-MUB and the loss converges well, as shown in Fig. 5, much higher than the traditional Pauli Z measurements. Empowered with PQEU, our ParaQuanNet demonstrates its superiority in efficiency compared with the existing quantum-classical hybrid models, as shown in Table 1. Parameter efficiency of our ParaQuanNet is enhanced dramatically compared to standard Quantum CNNs. Specifically, the number of parameters in our ParaQuanNet is around 29% of the number of parameters in QCNN, and the amount of samples being processed per second in our ParaQuanNet is 24 times of that in QCNN.

Algorithm 1 Quanvolution-based hybrid quantum–classical neural network

Initialize quantum device $\mathcal{Q}$ with n_{wires} qubits
Initialize quantum convolution kernel (parameterized quantum circuit) QLayer
Initialize a linear layer $W : \mathbb{R}^{64} \to \mathbb{R}^{8}$
for each input batch x with batch size B **do**
  Reshape each sample x into a 16×16 grid
  Initialize tensor patches $\in \mathbb{R}^{B\times 4\times 4\times 16}$
  for each patch row index c **do**
    for each patch column index r **do**
      Extract a 4×4 patch from rows $[c, c+4)$ and columns $[r, r+4)$
      Flatten each patch into a 16-dimensional vector and store in patches
    end
  end
  Reshape patches into a batch of patch vectors: patches $\in \mathbb{R}^{(B\cdot 16)\times 16}$
  Initialize the quantum device $\mathcal{Q}$ by encode the simulated quantum statevector into the quantum device via amplitude encoding.
  Apply QLayer on $\mathcal{Q}$
  if *measurement mode = 1* **then**
    Measure all qubits using M^Z and obtain feature matrix featureResult
  else
    if *measurement mode = 2* **then**
      Measure all qubits using M^X and obtain featureResult
    else
      Measure all qubits using M^Y and obtain featureResult
    end
  end
  Reshape measurement results into feature vectors: featureResult $\in \mathbb{R}^{B\times 64}$
  $y = W$featureResult $\in \mathbb{R}^{B\times 8}$
  Compute final prediction via log-softmax: $\hat{y} = \text{softmax}(y)$
end

The high classification accuracy demonstrate that even all the 8 generative circuits are trained to generate the same type of quantum data, but the corresponding quantum DDPM processes learned during the neural network training varies. Our PareQuanNet are effective method to learn the difference of these various quantum DDPM processes represented by the trained generative circuits.

To study the robustness of our ParaQuanNet, we consider two types of data noise, the single-qubit $R_x(\theta)$ noise and the depolarizing noise $\epsilon(\rho) = (1-p)\rho + \frac{p}{3}(\hat{X}\rho\hat{X} + \hat{Y}\rho\hat{Y} + \hat{Z}\rho\hat{Z})$, with $\hat{X}, \hat{Y}, \hat{Z}$ representing the Pauli operators. We artificially add these two types of noise to all the training data, and using these noised data to train our neural networks. And by adding the various level noise into our generated quantum data, we test our ParaQuanNet on its classification accuracy. As shown in Fig. 6, we see that both the classification accuracy

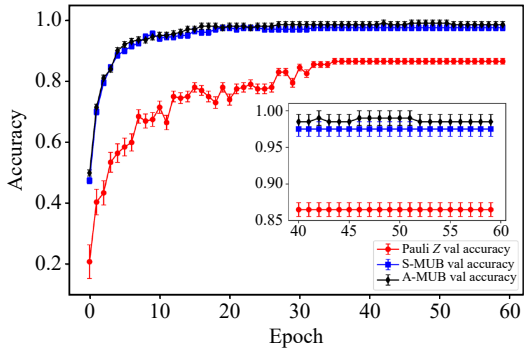

Fig. 5 The classification accuracy for the eight classes of quantum data.

Table 1 Quantum generative circuits classifications.

Method	QCNN	ParaQuanNet
Average accuracy	95%	99.5%
# of parameters	2194	637
Samples processed (s)	61	1011

of our ParaQuanNet and the data fidelity drop as the noise level increases.

Specifically, our ParaQuanNet performs well (with accuracy above 90%) while the $R_x(\theta)$ noise level is within $|\theta| < 0.1\pi$ and the depolarizing noise level is within $p < 0.02$. In contrast, the CNN method drops faster with the increase of noise level within the range where the classification accuracy is higher than 90%. The robustness of our method to the noise is consistent with the fidelity of the noise data still belonging to the W-like state group as shown in Fig. 6. As the fidelity of the noise data belonging to the W-like states drops, the identification accuracy of our method also drops, which is reasonable. We would like to emphasize that our ParaQuanNet is not only efficient in terms of data processing speed and the lower number of internet parameters, but also in the better robustness to the quantum-specialized noise types, such as the depolarizing noise. Specifically, with the increase of noise level, the classification accuracy of our ParaQuanNet drops much slower than CNN.

We further study the robustness of our approach by considering three types of realistic noisy cases, i.e. two-qubit gate fidelity, finite-shot measurement noise and readout errors.

Our approach performance considering single-qubit and two-qubit gate fidelity. The gate fidelity is one of the dominating issues in quantum computation. Our circuit is composite of single-qubit and two-qubit gates. Here we consider imperfect single-qubit and two qubit gates. Imperfect single-qubit gates are modeled using an equivalent parameterized $R_x(\theta)$ operator in the end of each qubit in our PQEU kernel. Imperfect two-

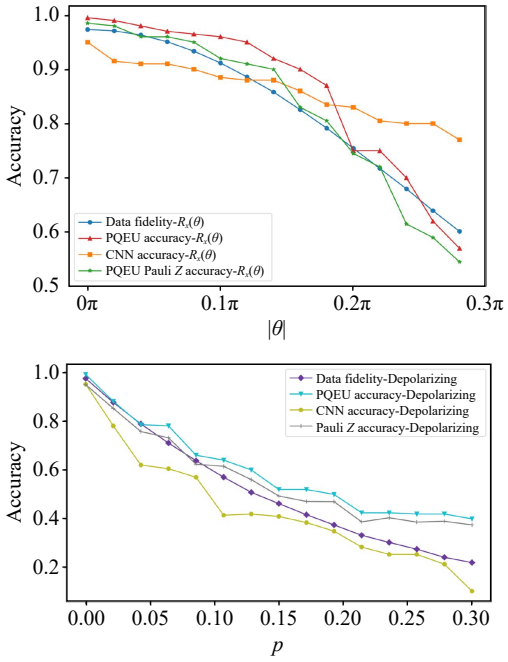

Fig. 6 The robustness of our ParaQuanNet to the $R_x(\theta)$ noise (top) and depolarizing noise $\epsilon(p)$ (bottom).

qubit entangling gates are modeled using a two-qubit depolarizing channel applied after each two-qubit operation (e.g., CNOT and controlled rotations):

$$\mathcal{E}_p^{(2)}(\rho) = (1 - p_{\text{gate}})\rho + p_{\text{gate}} I_4, \tag{3}$$

where p_{gate} denotes the depolarizing probability and I_4 is the 4×4 identity matrix. In simulation, this channel is implemented via a Pauli-twirled approximation,

$$\rho \mapsto (1 - p_{\text{gate}})\rho + \frac{p_{\text{gate}}}{15} \sum_{\substack{P,Q \in \{I,X,Y,Z\} \\ (P,Q) \neq (I,I)}} (P \otimes Q)\rho(P \otimes Q), \tag{4}$$

which provides a standard statevector-compatible approximation of two-qubit depolarizing noise.

As shown in Fig. 7, we implement our simulations under various gate fidelity level. In Fig. 7(a), we vary the parameter $\theta \in [0, 0.3\pi]$, we observe the robustness of our method to this single-qubit gate noise. We vary p_{gate} from to a realistic high value of 0.3 in Fig. 7(b). It is shown that our approach has a good robustness to the gate fidelity, the accuracy can reach 0.985 even at the depolarizing error $p_{\text{gate}} = 0.3$. We also witness that our S-MUB and A-MUB method outperform the standard the Pauli Z measurement method, demonstrate better robustness against the gate fidelity. In Fig. 7(c), we show the performance of our method while considering

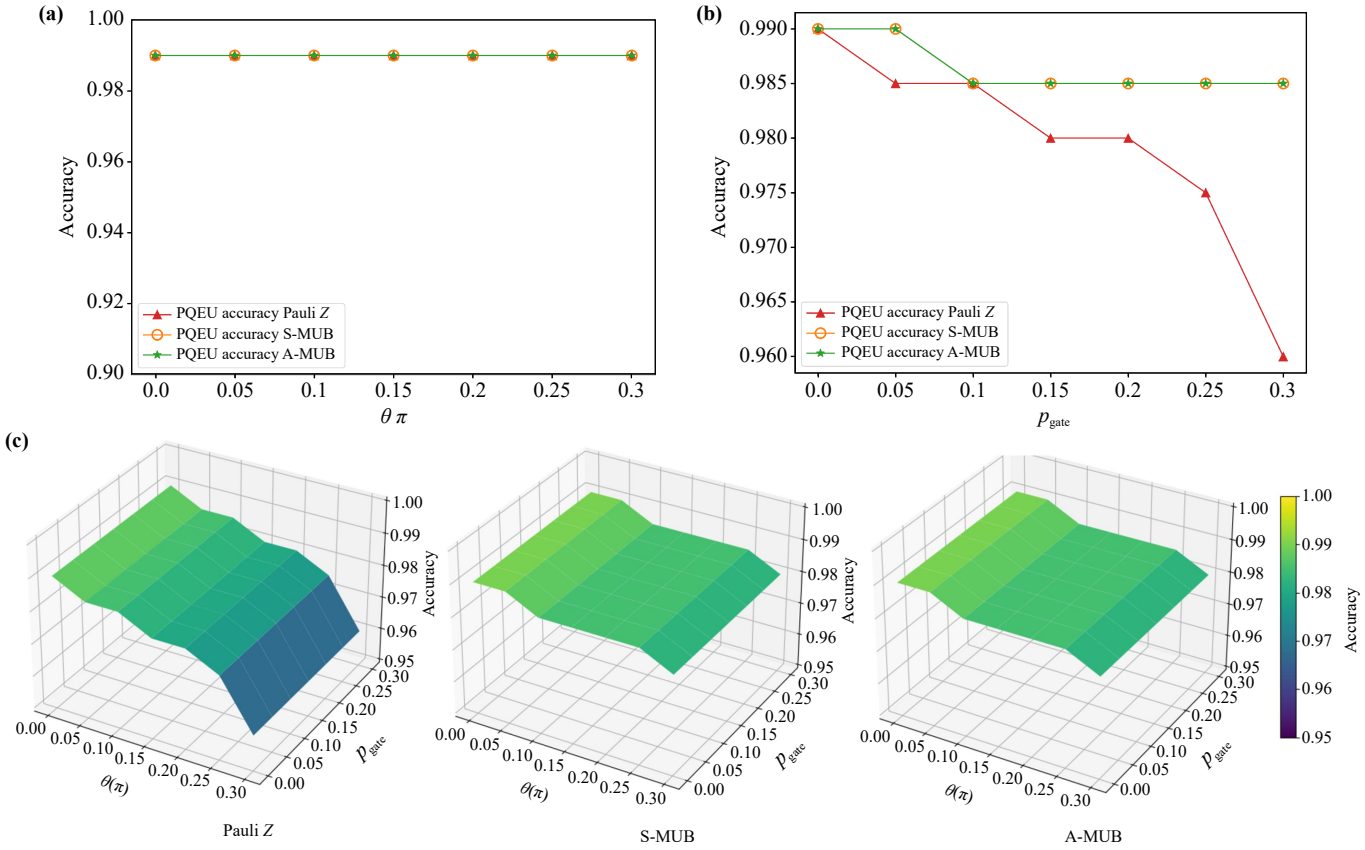

Fig. 7 Classification accuracy under **(a)** single-qubit gate noise, **(b)** two-qubit gate noise and **(c)** both single- and two-qubit gate noise under Pauli Z (left), S-MUB (center), A-MUB (right) measurement strategies.

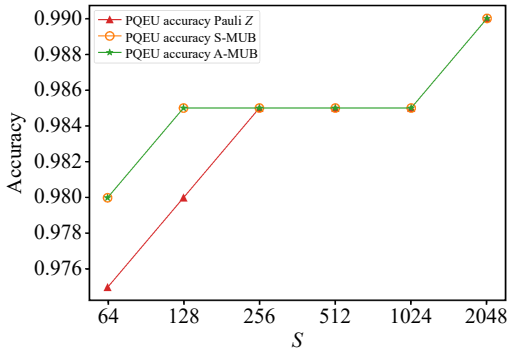

Fig. 8 Classification accuracy under finite-shot measurement noise.

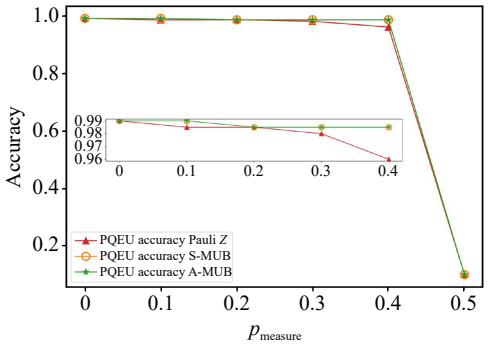

Fig. 9 Classification accuracy under measurement readout noise. The parameter p_{measure} denotes the probability of classical bit-flip error applied to each measurement outcome. An inset shows a magnified view for $p_{\text{measure}} \leq 0.4$. MUB-based strategies (S-MUB and A-MUB) demonstrate better robustness compared to single Pauli Z measurement.

both single-qubit and two-qubit gate noise, where left is Pauli Z measuremnt case, center is the S-MUB case, and right is the A-MUB case.

Finite-shot measurement noise. On quantum devices, Pauli expectation values are estimated using a finite number of shots S. If $\mu = \langle\sigma\rangle$ denotes the ideal expectation value, then the empirical estimator

$$\hat{\mu} = \frac{1}{S}\sum_{i=1}^{S} x_i, \qquad x_i \in \{+1, -1\}, \tag{5}$$

satisfies

$$\mathbb{E}[\hat{\mu}] = \mu, \qquad \text{Var}(\hat{\mu}) = \frac{1-\mu^2}{S}. \tag{6}$$

For moderate S, we adopt the Gaussian approximation

$$\hat{\mu} \sim \mathcal{N}\left(\mu, \frac{1-\mu^2}{S}\right), \tag{7}$$

which enables differentiable simulation of shot noise.

In Fig. 8, we show the accuracy improves with the number of measurements increase which is reasonable since more measurements provides more information on the quantum states.

Readout noise. Symmetric readout bit-flip noise with probability p_{measure} is added in our model as shown in Fig. 9. We observe that while $p_{\text{measure}} < 0.5$, our model is able to compensate the bit flip readout, and ensures a high classification accuracy above 0.98 for A-MUB strategy. While $p_{\text{measure}} = 0.5$, corresponding to fully random measurement outcomes, the classification fails as a expected since there is no information in the measurement outcomes.

We study the time complexity of traditional QCNN and PQEU considering the following ingredients: the number of rows N and columns M after gridding, the computational cost of a complete quantum stream T_{circ}, including encoding, circuit evolution, and measurement.

For the traditional QCNN, each of the $N \times M$ image patches must be encoded and processed by an independent quantum circuit. Therefore, the total complexity is

$$T_{\text{traditional}} = O(NM \cdot T_{\text{circ}}). \tag{8}$$

In contrast, our **PQEU** approach requires only parallel executions on multi copies of the PQEU, the time required is independent of N and M, but the numbe of the PQEU relies on the value of N and M. The classical simulation time complexity in our GPU platform is

$$T_{\text{PQEU}} = O(T_{\text{circ}}). \tag{9}$$

Our analysis shows that PQEU reduces the time cost dependence on the number of patches and achieves an asymptotic speedup of $O(NM)$ over the traditional QCNN with the cost of multi compies of PQEU. In practice, this implies that as the size of input data grows, the computational burden of the conventional QCNN increases quadratically with the number of patches, whereas PQEU maintains a constant overhead. Such scalability makes PQEU particularly advantageous for large-scale or high-dimensional quantum-enhanced learning tasks.

We study the scalability of our approach by considering increasing the size of each input data (input resolution), complexity of each data, and the total amount of data.

Increasing input complexity. When task complexity increases, the expressivity of the quantum kernel can be enhanced by moderately increasing the circuit depth, while keeping the qubit count. Since the PQEU functions as a localized convolutional kernel rather than a global variational circuit, increasing depth effectively improves feature extraction capacity without requiring additional qubits.

Increasing input resolution. For larger images of size $H \times W$, the number of patches

$$K = \frac{H}{p} \cdot \frac{W}{p}$$

Table 2 Comparison with recent representative quantum neural network approaches. Reported values are taken from original papers under their respective settings.

Method	MNIST	Fashion-MNIST
Quantum Deep Equilibrium Model [48]	73.7%	72.1%
Resource-Efficient QCNN [49]	92.3%	88.5%
ParaQuanNet (Ours)	96.5%	84.3%

increases, but the quantum kernel circuit remains identical. Thus, qubit count and circuit depth per patch remain constant. The resource overhead scales linearly with the number of patches, similar to classical convolutional networks.

Increasing the amount of data. When the dataset size increases, both the training and evaluation time scale approximately linearly with the number of samples. However, the computational complexity of a single forward inference remains unchanged, since the circuit structure and qubit count are fixed.

Overall, the scalability of our framework resembles classical convolutional architectures: dataset enlargement primarily increases patch training rather than circuit width, while increases in data complexity can be accommodated through moderate depth enhancement rather than drastic qubit expansion.

We also compare with two recent representative quantum(-hybrid) image-classification works (2024–2025) to show the efficiency of our approach as shown in Table 2.

2.5 Experimental settings

Our experimental model's hyperparameters were optimized through systematic grid searches and quantum hardware-aware tuning. Key configurations are shown in Table 3. The loss function in our experiments is the cross-entropy loss with L_2 regularization:

$$\mathcal{L} = -\sum_{c=1}^{C} y_c \log(\hat{y}_c).$$

All our experiments are simulated in calssical GPU. Our experiments are implemented on a computer configured with two AMD EPYC 9554 CPUs, four NVIDIA A100 GPUs, 512GB of memory, a Ubuntu 20.04 system, Python 3.8.13, and the torchquantum 0.1.5 framework.

Table 3 Optimized parameter settings.

Parameter	Value
Batch size	32
Optimizer	Adam
Learning rate	0.002
Epochs	40
Qubit	4
Simulation environment	TorchQuantum

Each experiment was verified five times. The seed value was set to [0, 1, 2, 3, 4] at the beginning of each experiment before the following operations: (i) dataset splitting, (ii) model weight initialization, and (iii) any stochastic data augmentation operations.

2.6 Classification of classical data with our ParaQuanNet

Our ParaQuanNet is also suitable for the classification tasks of classical data. To further validate the performance of the proposed ParaQuanNet model, we conducted additional experiments on several widely used benchmark datasets, including MNIST, Fashion-MNIST, EMNIST, and CIFAR-10. The classical data in Table 4 are encoded into quantum states via the amplitude encoding method in Ref. [50]. Then the encoded quantum states are fed into our ParaQuanNet for the training and test processes. The result is shown in Table 4. Our ParaQuanNet dramatically improves the classification accuracies compared with the conventional QCNN. Specifically, for MNIST, the accuracies are improved by $22.3\%, 10.5\%, 44.2\%, 16\%$ for each of the testing data set. And we also witness the accuracy improvement with our proposed MUB measurement methods.

3 Conclusion

In this work, we identify the quantum generative circuits for the quantum data copyright protection in the coming quantum AI era. We propose a PQEU model for the parallel quantum date processing in quantum neural networks and propose two mutual unbiased basis measurement methods to effectively improve the performance of our parallel neural network. The high identification accuracy of quantum generative circuits reveals

Table 4 Performance of the proposed PQEU model on benchmark datasets.

Method	**MNIST**	**Fashion-MNIST**	**EMNIST**	**CIFAR-10**
QCNN accuracy	74.2%	73.8%	34.4%	33.1%
PQEU accuracy	93.1%	82.3%	78.3%	44.3%
PQEU AND S-MUB accuracy	96.1%	83.3%	78.6%	47.9%
PQEU AND A-MUB accuracy	96.5%	84.3%	78.6%	49.1%
Accuracy improvement	22.3%	10.5%	44.2%	16%

that the various quantum DDPM processes inherit the different quantum space mappings, which is the key that our ParaQuanNet learns. Our approach is robustness to the data noise and the circuit level noise, which enable its applicaiton on NISQ devices. Our proposed method also applies to the classification tasks of classical data sets and the performance is much higher than conventional quantum neural networks. Our results demonstrate that ParaQuanNet offers a scalable and effective framework for the reliable identification of quantum circuits, enabling more accurate characterization of quantum generative models and strengthening the foundations for interpretable, verifiable, and ultimately quantum machine intelligence.

Declarations The authors declare that they have no competing interests and there are no conflicts.

Acknowledgements We acknowledge support from the National Natural Science Foundation of China (Grant No. 62571434) and the Fundamental Research Funds for the Central Universities.

References

1. S. K. Liao, W. Q. Cai, W. Y. Liu, L. Zhang, Y. Li, et al., Satellite-to-ground quantum key distribution, *Nature* 549(7670), 43 (2017)
2. A. S. Cacciapuoti, M. Caleffi, F. Tafuri, F. S. Cataliotti, S. Gherardini, and G. Bianchi, Quantum internet: Networking challenges in distributed quantum computing, *IEEE Netw.* 34(1), 137 (2020)
3. Y. Li, W. Q. Cai, J. G. Ren, C. Z. Wang, M. Yang, et al., Microsatellite-based real-time quantum key distribution, *Nature* 640, 47 (2025)
4. F. Arute, K. Arya, R. Babbush, D. Bacon, J. C. Bardin, R. Barends, et al., Quantum supremacy using a programmable superconducting processor, *Nature* 574(7779), 505 (2019)
5. H. S. Zhong, H. Wang, Y. H. Deng, M. C. Chen, L. C. Peng, Y. H. Luo, J. Qin, D. Wu, X. Ding, Y. Hu, P. Hu, X. Y. Yang, W. J. Zhang, H. Li, Y. Li, X. Jiang, L. Gan, G. Yang, L. You, Z. Wang, L. Li, N. L. Liu, C. Y. Lu, and J. W. Pan, Quantum computational advantage using photons, *Science* 370(6523), 1460 (2020)
6. S. Krinner, N. Lacroix, A. Remm, A. Di Paolo, E. Genois, C. Leroux, C. Hellings, S. Lazar, F. Swiadek, J. Herrmann, G. J. Norris, C. K. Andersen, M. Müller, A. Blais, C. Eichler, and A. Wallraff, Realizing repeated quantum error correction in a distance-three surface code, *Nature* 605(7911), 669 (2022)
7. H. Gao, L. S. Martin, L. B. Hughes, N. T. Leitao, P. Put, H. Zhou, N. U. Koyluoglu, S. A. Meynell, A. C. B. Jayich, H. Park, and M. D. Lukin, Signal amplification in a solid-state sensor through asymmetric many-body echo, *Nature* 646(8083), 68 (2025)
8. P. J. O'Malley, R. Babbush, I. D. Kivlichan, J. Romero, J. R. McClean, et al., Scalable quantum simulation of molecular energies, *Phys. Rev. X* 6(3), 031007 (2016)
9. J. Argüello-Luengo, A. González-Tudela, T. Shi, P. Zoller, and J. I. Cirac, Analogue quantum chemistry simulation, *Nature* 574(7777), 215 (2019)
10. C. Doyle, W. W. Zhang, M. Wang, B. A. Bell, S. D. Bartlett, and A. Blanco-Redondo, Biphoton entanglement of topologically distinct modes, *Phys. Rev. A* 105(2), 023513 (2022)
11. A. D. King, A. Nocera, M. M. Rams, J. Dziarmaga, R. Wiersema, et al., Beyond-classical computation in quantum simulation, *Science* 388(6743), 199 (2025)
12. W. W. Zhang, Z. Wu, H. Jia, W. Zhao, Q. Ji, W. Pan, and H. Shi, Quantum versatility in pagerank, *Phys. Rev. Res.* 6(4), 043163 (2024)
13. W. W. Zhang, C. Chen, and J. Wu, Self-induced manipulation of biphoton entanglement in topologically distinct modes, *Phys. Rev. Appl.* 24(5), 054025 (2025)
14. V. Giovannetti, S. Lloyd, and L. Maccone, Quantum metrology, *Phys. Rev. Lett.* 96(1), 010401 (2006)
15. W. Dür, M. Skotiniotis, F. Fröwis, and B. Kraus, Improved quantum metrology using quantum error correction, *Phys. Rev. Lett.* 112(8), 080801 (2014)
16. V. Montenegro, C. Mukhopadhyay, R. Yousefjani, S. Sarkar, U. Mishra, M. G. Paris, and A. Bayat, Review: Quantum metrology and sensing with many-body systems, *Phys. Rep.* 1134, 1 (2025)
17. M. Fadel, N. Roux, and M. Gessner, Quantum metrology with a continuous-variable system, *Rep. Prog. Phys.* 88(10), 106001 (2025)
18. S. Chen, J. Cotler, H. Y. Huang, and J. Li, The complexity of NISQ, *Nat. Commun.* 14(1), 6001 (2023)
19. J. W. Z. Lau, K. H. Lim, H. Shrotriya, and L. C. Kwek, NISQ computing: where are we and where do we go? *AAPPS Bulletin* 32, 27 (2022)
20. J. Ho, A. Jain, and P. Abbeel, Denoising diffusion probabilistic models, arXiv: 2006.11239v2 (2020)
21. B. Sanchez-Lengeling and A. Aspuru-Guzik, Inverse molecular design using machine learning: Generative models for matter engineering, *Science* 361(6400), 360 (2018)
22. I. Goodfellow, J. Pouget-Abadie, M. Mirza, B. Xu, D. Warde-Farley, S. Ozair, A. Courville, and Y. Bengio, Generative adversarial networks, *Commun. ACM* 63(11), 139 (2020)
23. J. Wei, Y. Tay, R. Bommasani, C. Raffel, B. Zoph, et al., Emergent abilities of large language models, arXiv: 2206.07682 (2022)
24. S. R. Bowman, Eight things to know about large language models, arXiv: 2304.00612 (2023)
25. S. Bubeck, V. Chandrasekaran, R. Eldan, J. Gehrke, E. Horvitz, et al., Sparks of artificial general intelligence: Early experiments with gpt-4, arXiv: 2303.12712 (2023)
26. G. Sastry, L. Heim, H. Belfield, M. Anderljung, M. Brundage, et al., Computing power and the governance of artificial intelligence, arXiv: 2402.08797 (2024)
27. A. Kandala, A. Mezzacapo, K. Temme, M. Takita, M. Brink, J. M. Chow, and J. M. Gambetta, Hardware-efficient variational quantum eigensolver for small molecules and quantum magnets, *Nature* 549, 242 (2017)
28. M. Cerezo, A. Arrasmith, R. Babbush, S. C. Benjamin, S. Endo, K. Fujii, J. R. McClean, K. Mitarai, X. Yuan,

L. Cincio, and P. J. Coles, Variational quantum algorithms, *Nat. Rev. Phys.* 3(9), 625 (2021)
29. N. A. Nghiem, S. Y. C. Chen, and T. C. Wei, Unified framework for quantum classification, *Phys. Rev. Res.* 3(3), 033056 (2021)
30. T. Hur, L. Kim, and D. K. Park, Quantum convolutional neural network for classical data classification, *Quantum Mach. Intell.* 4(1), 3 (2022)
31. M. Kölle, G. Stenzel, J. Stein, S. Zielinski, B. Ommer, and C. Linnhoff-Popien, Quantum denoising diffusion models, in: 2024 IEEE International Conference on Quantum Software (QSW), IEEE, 2024, pp 88–98
32. R. Wang, Y. Wang, J. Liu, and T. Koike-Akino, Quantum diffusion models for few-shot learning, arXiv: 2411.04217 (2024)
33. S. Minami, K. Nakaji, Y. Suzuki, A. Aspuru-Guzik, and T. Kadowaki, Generative quantum combinatorial optimization by means of a novel conditional generative quantum eigensolver, arXiv: 2501.16986 (2025)
34. W. W. Zhang, X. Huang, S. Shan, W. Zhao, B. Yang, W. Pan, and H. Shi, Quantum data generation in a denoising model with multiscale entanglement renormalization network, *Phys. Scr.* 100(6), 065120 (2025)
35. T. Shaik, X. Tao, H. Xie, and R. Sang, Quantum machine unlearning: Foundations, mechanisms, and taxonomy, arXiv: 2511.00406 (2025)
36. M. Parigi, S. Martina, and F. Caruso, Quantum-noise driven generative diffusion models, *Adv. Quantum Technol.* 8(12), 2300401 (2024)
37. B. Zhang, P. Xu, X. Chen, and Q. Zhuang, Generative quantum machine learning via denoising diffusion probabilistic models, *Phys. Rev. Lett.* 132(10), 100602 (2024)
38. G. Kwun, B. Zhang, and Q. Zhuang, Mixed-state quantum denoising diffusion probabilistic model, *Phys. Rev. A* 111(3), 032610 (2025)
39. G. P. He, Using a single circuit to compute the gradients with respect to all parameters of a quantum neural network, *Front. Phys. (Beijing)* 21(8), 083201 (2026)
40. Y. Liu, F. Meng, L. Wang, Y. Hu, Z. Zhang, and X. Yu, Output prediction of quantum circuits based on graph neural networks, *Front. Phys. (Beijing)* 21(6), 063201 (2026)
41. I. Cong, S. Choi, and M. D. Lukin, Quantum convolutional neural networks, *Nat. Phys.* 15(12), 1273 (2019)
42. Y. Wang, S. Chen, J. Wan, J. Meng, K. Zhang, W. Liu, and X. Ning, A multiple simd, multiple data (msmd) architecture: Parallel execution of dynamic and static simd fragments, in: 2013 IEEE 19th International Symposium on High Performance Computer Architecture (HPCA), IEEE, 2013, pp 603–614
43. N. Bent, H. Qassim, A. Tahir, D. Sych, G. Leuchs, L. L. Sánchez-Soto, E. Karimi, and R. Boyd, Experimental realization of quantum tomography of photonic qudits via symmetric informationally complete positive operator-valued measures, *Phys. Rev. X* 5(4), 041006 (2015)
44. A. Zhang, Y. Zhang, F. Xu, L. Li, and L. Zhang, Adaptive tomography of qubits: purity versus statistical fluctuations, *J. Phys. A Math. Theor.* 51(39), 395304 (2018)
45. S. Designolle, P. Skrzypczyk, F. Fröwis, and N. Brunner, Quantifying measurement incompatibility of mutually unbiased bases, *Phys. Rev. Lett.* 122(5), 050402 (2019)
46. A. Tavakoli, M. Farkas, D. Rosset, J. D. Bancal, and J. Kaniewski, Mutually unbiased bases and symmetric informationally complete measurements in bell experiments, *Sci. Adv.* 7(7), eabc3847 (2021)
47. M. Farkas, J. Kaniewski, and A. Nayak, Mutually unbiased measurements, hadamard matrices, and superdense coding, *IEEE Trans. Inf. Theory* 69(6), 3814 (2023)
48. P. Schleich, M. Skreta, L. B. Kristensen, R. Vargas-Hernandez, and A. Aspuru-Guzik, Quantum deep equilibrium models, *Adv. Neural Inf. Process. Syst.* 37, 31940 (2024)
49. Y. Song, J. Li, Y. Wu, S. Qin, Q. Wen, and F. Gao, A resource-efficient quantum convolutional neural network, *Front. Phys. (Lausanne)* 12, 1362690 (2024)
50. M. Rath, and H. Date, Quantum data encoding: A comparative analysis of classical-to-quantum mapping techniques and their impact on machine learning accuracy, *EPJ Quantum Technol.* 11(1), 72 (2024)